

Chemical and physical properties of complex perovskites in the $\text{La}_{0.8}\text{Sr}_{0.2}\text{MnO}_{3-\delta}-\text{La}_{0.8}\text{Sr}_{0.2}\text{CuO}_{2.4+\delta}-\text{La}_{0.8}\text{Sr}_{0.2}\text{FeO}_{3-\delta}$ system

Mohsine Zahid^{a,b}, Irudayam Arul Raj^c, Frank Tietz^{a,*}, Detlev Stöver^a

^a Institute of Energy Research (IEF-1), Forschungszentrum Jülich, D-52425 Jülich, Germany

^b European Institute for Energy Research, Emmy-Noether-Strasse 11, D-76131 Karlsruhe, Germany

^c Central Electrochemical Research Institute, Karaikudi 630006, India

Received 2 May 2007; accepted 9 May 2007

Available online 16 May 2007

Abstract

Perovskites resulting from discrete changes in composition within the quasi-ternary system $\text{La}_{0.8}\text{Sr}_{0.2}\text{MnO}_{3-\delta}-\text{La}_{0.8}\text{Sr}_{0.2}\text{CuO}_{2.4+\delta}-\text{La}_{0.8}\text{Sr}_{0.2}\text{FeO}_{3-\delta}$ were investigated under constant experimental conditions with the objective of obtaining an overview of the variation of the properties relevant for possible future applications. Nineteen nominal perovskite compositions within this system were systematically selected and synthesized under identical conditions by the Pechini method. The experimental data obtained on quantitative chemical analysis, powder X-ray diffraction, electrical conductivity and thermal expansion are presented collectively for the first time to facilitate comparisons. The formation and distribution of the different crystallographic phases at 950 °C within this quasi-ternary system are shown. The DC electrical conductivity is strongly influenced by the Cu content and increases up to 276 S cm^{-1} for $\text{La}_{0.8}\text{Sr}_{0.2}\text{CuO}_{2.4+\delta}$. The thermal expansion is dominated by the Cu/Mn ratio and is almost independent of the Fe content.

© 2007 Elsevier Masson SAS. All rights reserved.

Keywords: Perovskites; SOFC; Electrical conductivity; Thermal expansion

1. Introduction

A number of partially substituted perovskite systems with the general formula $\text{A}_{1-x}\text{A}'_x\text{B}_{1-y}\text{B}'_y\text{O}_3$ exhibit both electronic and mixed conductivity as a function of composition, making them useful for application either as a cathode or as contact layer material between the cathode and ferritic steel interconnect in planar solid oxide fuel cells (SOFCs) operating in the temperature range of 700–800 °C [1–7]. Crystallographic stability, adequate DC electrical conductivity levels and compatible coefficients of thermal expansion are mandatory for such applications. $\text{La}_{1-x}\text{Sr}_x\text{CuO}_{2.4+\delta}$ has been studied for its application as a high-temperature superconducting material [8,9] and also as a cathode in SOFCs [9]. It is reported that the stabilization of multivalent copper ions in the perovskite lattice is critical in order to achieve physical and chemical properties

suitable for these applications [10,11]. Very recently Zahid et al. [12] investigated in detail the high-temperature properties of $\text{La}_{0.8}\text{Sr}_{0.2}\text{CuO}_{2.4+\delta}$ and found that the material is applicable for SOFCs as long as the temperature during assembly and operation is maintained below about 1000 °C. Because only very small amounts of oxygen release have been found at $T \leq 1000$ °C for $\text{La}_{0.8}\text{Sr}_{0.2}\text{MnO}_{3-\delta}$ [13], $\text{La}_{0.8}\text{Sr}_{0.2}\text{FeO}_{3-\delta}$ [1] and $\text{La}_{0.8}\text{Sr}_{0.2}\text{CuO}_{2.4+\delta}$ [10,12], the influence of the oxygen content on physical properties below 1000 °C seems to be negligible also for the other compositions in the quasi-ternary system and, taking into account the small non-stoichiometry of oxygen, the general formula of the investigated system is more precisely described as $\text{La}_{0.8}\text{Sr}_{0.2}\text{Mn}_{1-x-y}\text{Fe}_x\text{Cu}_y\text{O}_{2.9-y/2+\delta}$ with $0.04 < \delta < 0.1$ [1,10,12–14].

Partial substitution of Cu by Mn and/or Fe in this perovskite is expected to change the properties relevant for SOFC application. Many investigations have been carried out on perovskites with Mn or Fe on the B-site to characterize their properties, for example see Refs. [1–5,7,13,15]. However, a review of the published results on these compositions revealed

* Corresponding author. Tel.: +49 2461 615007; fax: +49 2461 612455.

E-mail address: f.tietz@fz-juelich.de (F. Tietz).

that different authors adopt different synthesis, processing and measurement procedures, thereby reporting data with significant variations (e.g. for $\text{La}_{1-x}\text{Sr}_x\text{CoO}_{3-\delta}$ see Ref. [3]). This makes it difficult to compare the properties of different compositions within the same system. Although several reports are available on the systematic evaluation of properties for single series of compositions within the $\text{La}_{0.8}\text{Sr}_{0.2}\text{MnO}_{3-\delta}$ – $\text{La}_{0.8}\text{Sr}_{0.2}\text{CuO}_{2.4+\delta}$ – $\text{La}_{0.8}\text{Sr}_{0.2}\text{FeO}_{3-\delta}$ system, no attempt has been previously made to synthesize several series of compositions under identical conditions thus making it possible to have a complete set of data for various properties within the whole quasi-ternary system. The objective of the present work is to give an overview of the formation and distribution of different crystallographic phases at different temperatures and the dependence of electrical conductivity, as well as thermal expansion, on temperature and composition.

2. Experimental

Systematically selected compositions in the quasi-ternary system $\text{La}_{0.8}\text{Sr}_{0.2}\text{MnO}_{3-\delta}$ – $\text{La}_{0.8}\text{Sr}_{0.2}\text{CuO}_{2.4+\delta}$ – $\text{La}_{0.8}\text{Sr}_{0.2}\text{FeO}_{3-\delta}$ were synthesized by the Pechini method using nitrate solutions of La, Sr, Mn, Fe and Cu in the corresponding cation ratios. A detailed description of the synthesis process is given previously [7,12,16].

After calcination at 600 °C for 3 h in air, the resulting raw powders were analytically investigated by inductively coupled plasma atomic emission spectrometry (ICP-AES) performed on aqueous solutions obtained by dissolving the powders in nitric acid to determine the elemental composition.

Additionally, a sample of each prepared powder was heat-treated at 950 °C for 6 h. The crystallographic phases of these samples were determined by X-ray diffraction (XRD) analysis using a Siemens D5000 diffractometer and $\text{Cu K}\alpha$ radiation. The raw powders calcined at 600 °C were uniaxially pressed

to form bars ($40 \times 5 \times 4 \text{ mm}^3$) and sintered at 950 °C for 6 h. The total electrical conductivity of the sintered samples was measured by a four-probe DC technique at temperatures between 100 °C and 900 °C in air using silver wires and silver paste as contacts. The thermal expansion between room temperature and 900 °C was determined using a Netzsch DIL 402C dilatometer.

3. Results and discussion

3.1. Chemical and XRD analyses

The results obtained from the quantitative elemental analysis of the synthesized powders were normalized to 2 mol of cations per formula unit and showed no significant deviations from the nominal compositions (Table 1). The changes observed in the stoichiometric ratio are very close to the detection limits ($\pm 3\%$) of the ICP-AES.

The XRD results of the samples heat-treated at 950 °C for 6 h, summarized in Table 2, reveal that the perovskite structure was obtained as the main phase in most cases, crystallizing in the orthorhombic, tetragonal or hexagonal modification. Only in samples 001, 010 and 011 were impurities detected. This is due to the low sintering temperature of these samples as already discussed in Ref. [7]. The crystallographic structure of the compositions along the quasi-binary system $\text{La}_{0.8}\text{Sr}_{0.2}\text{MnO}_{3-\delta}$ – $\text{La}_{0.8}\text{Sr}_{0.2}\text{FeO}_{3-\delta}$ was previously discussed in detail [7,14].

The results of the XRD analysis indicate that the quasi-ternary diagram shown in Fig. 1 can be schematically subdivided into seven regions:

- The (P_{tet}) region located at the $\text{La}_{0.8}\text{Sr}_{0.2}\text{CuO}_{2.4+\delta}$ vertex is characterized by the presence of the tetragonal perovskite structure as the only phase detected.

Table 1
Compositions of the synthesized powders

Sample number	Nominal composition	Analytical composition ^a
001	$\text{La}_{0.8}\text{Sr}_{0.2}\text{MnO}_{3-\delta}$	$\text{La}_{0.809}\text{Sr}_{0.196}\text{Mn}_{0.995}\text{O}_{2.902+\delta}$
020	$\text{La}_{0.8}\text{Sr}_{0.2}\text{Mn}_{0.75}\text{Cu}_{0.25}\text{O}_{2.775+\delta}$	$\text{La}_{0.817}\text{Sr}_{0.198}\text{Mn}_{0.733}\text{Cu}_{0.252}\text{O}_{2.775+\delta}$
021	$\text{La}_{0.8}\text{Sr}_{0.2}\text{Mn}_{0.5}\text{Cu}_{0.5}\text{O}_{2.65+\delta}$	$\text{La}_{0.801}\text{Sr}_{0.200}\text{Mn}_{0.49}\text{Cu}_{0.509}\text{O}_{2.646+\delta}$
022	$\text{La}_{0.8}\text{Sr}_{0.2}\text{Mn}_{0.25}\text{Cu}_{0.75}\text{O}_{2.525+\delta}$	$\text{La}_{0.799}\text{Sr}_{0.198}\text{Mn}_{0.250}\text{Cu}_{0.754}\text{O}_{2.526+\delta}$
023	$\text{La}_{0.8}\text{Sr}_{0.2}\text{CuO}_{2.4+\delta}$	$\text{La}_{0.791}\text{Sr}_{0.199}\text{Cu}_{1.011}\text{O}_{2.397+\delta}$
024	$\text{La}_{0.8}\text{Sr}_{0.2}\text{Cu}_{0.75}\text{Fe}_{0.25}\text{O}_{2.525+\delta}$	$\text{La}_{0.788}\text{Sr}_{0.198}\text{Cu}_{0.768}\text{Fe}_{0.246}\text{O}_{2.517+\delta}$
025	$\text{La}_{0.8}\text{Sr}_{0.2}\text{Cu}_{0.5}\text{Fe}_{0.5}\text{O}_{2.65+\delta}$	$\text{La}_{0.817}\text{Sr}_{0.196}\text{Cu}_{0.500}\text{Fe}_{0.487}\text{O}_{2.652+\delta}$
026	$\text{La}_{0.8}\text{Sr}_{0.2}\text{Cu}_{0.25}\text{Fe}_{0.75}\text{O}_{2.775+\delta}$	$\text{La}_{0.807}\text{Sr}_{0.200}\text{Cu}_{0.251}\text{Fe}_{0.742}\text{O}_{2.775+\delta}$
009	$\text{La}_{0.8}\text{Sr}_{0.2}\text{FeO}_{3-\delta}$	$\text{La}_{0.799}\text{Sr}_{0.191}\text{Fe}_{1.011}\text{O}_{2.906+\delta}$
010	$\text{La}_{0.8}\text{Sr}_{0.2}\text{Fe}_{0.75}\text{Mn}_{0.25}\text{O}_{2.525+\delta}$	$\text{La}_{0.809}\text{Sr}_{0.191}\text{Fe}_{0.748}\text{Mn}_{0.252}\text{O}_{2.905+\delta}$
011	$\text{La}_{0.8}\text{Sr}_{0.2}\text{Fe}_{0.5}\text{Mn}_{0.5}\text{O}_{3-\delta}$	$\text{La}_{0.812}\text{Sr}_{0.191}\text{Fe}_{0.501}\text{Mn}_{0.496}\text{O}_{2.905+\delta}$
012	$\text{La}_{0.8}\text{Sr}_{0.2}\text{Fe}_{0.25}\text{Mn}_{0.75}\text{O}_{3-\delta}$	$\text{La}_{0.813}\text{Sr}_{0.195}\text{Fe}_{0.254}\text{Mn}_{0.739}\text{O}_{2.904+\delta}$
027	$\text{La}_{0.8}\text{Sr}_{0.2}\text{Cu}_{0.75}\text{Fe}_{0.125}\text{Mn}_{0.125}\text{O}_{2.525+\delta}$	$\text{La}_{0.809}\text{Sr}_{0.193}\text{Cu}_{0.756}\text{Fe}_{0.12}\text{Mn}_{0.122}\text{O}_{2.526+\delta}$
028	$\text{La}_{0.8}\text{Sr}_{0.2}\text{Cu}_{0.5}\text{Fe}_{0.25}\text{Mn}_{0.25}\text{O}_{2.65+\delta}$	$\text{La}_{0.809}\text{Sr}_{0.197}\text{Cu}_{0.507}\text{Fe}_{0.244}\text{Mn}_{0.243}\text{O}_{2.648+\delta}$
029	$\text{La}_{0.8}\text{Sr}_{0.2}\text{Cu}_{0.25}\text{Fe}_{0.375}\text{Mn}_{0.375}\text{O}_{2.775+\delta}$	$\text{La}_{0.817}\text{Sr}_{0.197}\text{Cu}_{0.252}\text{Fe}_{0.365}\text{Mn}_{0.369}\text{O}_{2.776+\delta}$
030	$\text{La}_{0.8}\text{Sr}_{0.2}\text{Cu}_{0.25}\text{Fe}_{0.5625}\text{Mn}_{0.1875}\text{O}_{2.775+\delta}$	$\text{La}_{0.809}\text{Sr}_{0.198}\text{Cu}_{0.255}\text{Fe}_{0.555}\text{Mn}_{0.183}\text{O}_{2.774+\delta}$
031	$\text{La}_{0.8}\text{Sr}_{0.2}\text{Cu}_{0.5}\text{Fe}_{0.375}\text{Mn}_{0.125}\text{O}_{2.65+\delta}$	$\text{La}_{0.808}\text{Sr}_{0.197}\text{Cu}_{0.504}\text{Fe}_{0.369}\text{Mn}_{0.122}\text{O}_{2.65+\delta}$
032	$\text{La}_{0.8}\text{Sr}_{0.2}\text{Cu}_{0.25}\text{Fe}_{0.1875}\text{Mn}_{0.5625}\text{O}_{2.775+\delta}$	$\text{La}_{0.809}\text{Sr}_{0.199}\text{Cu}_{0.257}\text{Fe}_{0.187}\text{Mn}_{0.548}\text{O}_{2.772+\delta}$
033	$\text{La}_{0.8}\text{Sr}_{0.2}\text{Cu}_{0.5}\text{Fe}_{0.125}\text{Mn}_{0.375}\text{O}_{2.65+\delta}$	$\text{La}_{0.813}\text{Sr}_{0.196}\text{Cu}_{0.499}\text{Fe}_{0.123}\text{Mn}_{0.369}\text{O}_{2.653+\delta}$

^a The oxygen content was calculated according to the cation contents.

Table 2
Crystalline phases observed after sintering at 950 °C for 6 h in air

Sample number	Crystallographic phases after calcination at 950 °C for 6 h	Lattice parameters of the main perovskite phase		
		<i>a</i>	<i>b</i>	<i>c</i>
001	P _{hex} + La ₂ O ₃	5.511(2)	—	13.346(8)
020	P _{hex}	5.507(2)	—	13.303(7)
021	P _{hex}	5.490(2)	—	13.293(7)
022	P _{tetr+hex}	10.761(23)	—	3.882(14)
023	P _{tetr}	10.842(4)	—	3.855(2)
024	P _{tetr+hex}	10.783(4)	—	3.902(3)
025	P _{hex+tetr}	5.522(4)	—	13.436(16)
026	P _{hex+tetr}	5.515(4)	—	13.440(14)
009	P _{or}	5.548(2)	5.519(2)	7.817(5)
010	P _{or} + La ₂ O ₃	5.540(5)	5.512(6)	7.788(9)
011	P _{or} + La ₂ O ₃	5.537(2)	5.492(3)	7.786(4)
012	P _{hex}	5.522(2)	—	13.369(8)
027	P _{tetr+hex}	10.770(8)	—	3.900(7)
028	P _{hex+tetr}	5.500(11)	—	13.317(17)
029	P _{hex}	5.513(2)	—	13.343(7)
030	P _{hex}	5.513(2)	—	13.345(7)
031	P _{hex+tetr}	5.504(7)	—	13.362(23)
032	P _{hex}	5.510(2)	—	13.321(7)
033	P _{hex+tetr}	5.491(5)	—	13.306(17)

- (P_{tetr+hex}) shows the tetragonal perovskite structure as the main phase and a hexagonal perovskite as the secondary phase.
- (P_{hex+tetr}) shows the hexagonal perovskite structure as the predominant phase and a tetragonal perovskite as the secondary phase.
- (P_{hex}), covering the central region of the diagram, shows only the hexagonal perovskite structure.

- The (P_{hex}) + La₂O₃ region is similar to the previous one, but contains small amounts of La₂O₃ as an impurity.
- (P_{orth}) located at the La_{0.8}Sr_{0.2}FeO_{3-δ} vertex reveals the orthorhombic perovskite structure.
- (P_{orth}) + La₂O₃ represents the region where the main orthorhombic phase is accompanied by small amounts of La₂O₃ as an impurity.

The XRD patterns of the series La_{0.8}Sr_{0.2}Cu_{1-2x}Mn_xFe_xO_{2.4+x+δ} (*x* = 0, 0.125, 0.25, 0.375 and 0.5) presented in Fig. 2 show the various crystal phases obtained after heat treatment at 950 °C depending on the composition. La_{0.8}Sr_{0.2}Mn_{0.5}Fe_{0.5}O_{3-δ} (sample 011) crystallizes as an orthorhombic perovskite (filled circles) with a small amount of La₂O₃ as an impurity, not visible in the XRD segment shown in Fig. 2. The addition of Cu (*x* = 0.125) in sample 029 leads to the disappearance of the orthorhombic structure and the crystallization of the single-phase hexagonal perovskite (filled stars). At *x* = 0.25 (sample 028) a tetragonal perovskite can also be detected as a secondary crystalline phase (open circles). A further increase of the Cu content (*x* = 0.375, sample 027) is accompanied by a decrease in intensity of the reflections of the hexagonal perovskite phase. The tetragonal perovskite becomes the dominant phase. For La_{0.8}Sr_{0.2}CuO_{2.4+δ} (sample 023) only the tetragonal perovskite was detected.

3.2. Electrical conductivity

Because sintering was carried out at 950 °C to avoid melting of the Cu-rich samples, all specimens remained porous (see Table 3).

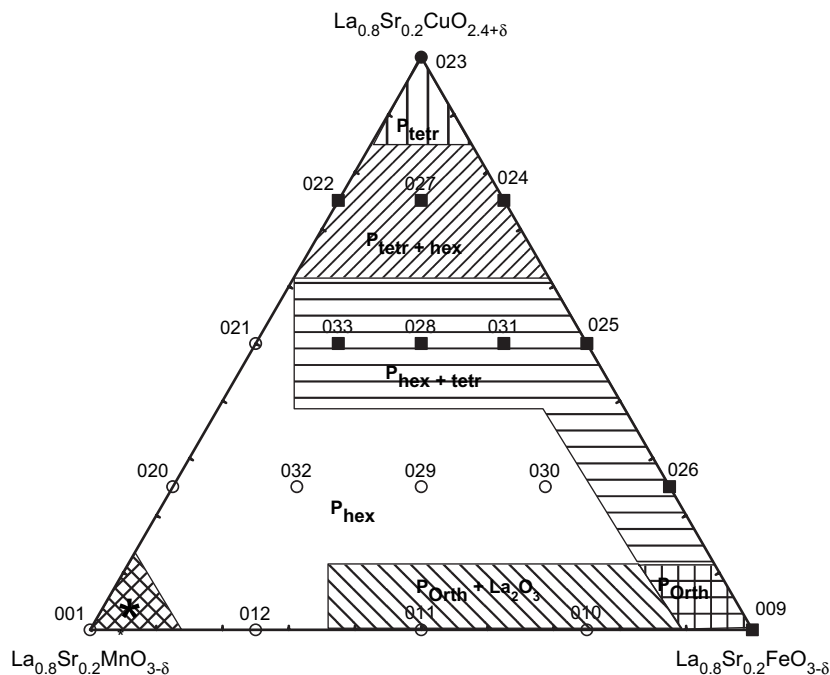


Fig. 1. Schematic overview of the distribution of the main and secondary crystallographic phases within the quasi-ternary La_{0.8}Sr_{0.2}MnO_{3-δ}–La_{0.8}Sr_{0.2}CuO_{2.4+δ}–La_{0.8}Sr_{0.2}FeO_{3-δ} system after sintering at 950 °C in air. (*)Sample 001 contains P_{hex} + La₂O₃. The symbols indicate regimes with different behavior in electrical conductivity (see Table 3 and Fig. 4).

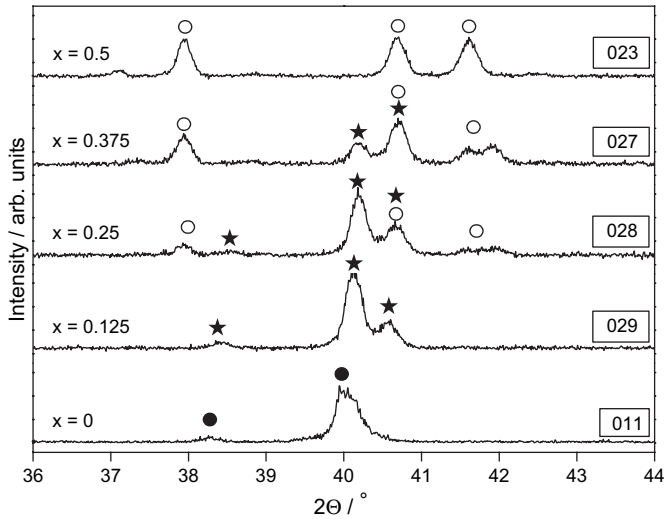


Fig. 2. Part of the XRD patterns between $36^\circ < 2\theta < 44^\circ$ of the compositions of the $\text{La}_{0.8}\text{Sr}_{0.2}\text{Cu}_{1-2x}\text{Mn}_x\text{Fe}_x\text{O}_{2.4+x+\delta}$ series ($x = 0, 0.125, 0.25, 0.375$ and 0.5) after calcination at 950°C for 6 h in air.

Therefore the conductivity data (σ) were corrected as described in Ref. [7] by applying the empirical formula:

$$\sigma_{\text{corrected}} = \sigma_{\text{measured}} / (1 - (p/100))^2 \quad (1)$$

with p = porosity (in %). The parameters of the electrical conductivity of the synthesized compositions in the $\text{La}_{0.8}\text{Sr}_{0.2}\text{MnO}_{3-\delta}$ – $\text{La}_{0.8}\text{Sr}_{0.2}\text{CuO}_{2.4+\delta}$ – $\text{La}_{0.8}\text{Sr}_{0.2}\text{FeO}_{3-\delta}$ system are summarized in Table 3. The electrical conductivity (σ) at 800°C varies by two orders of magnitude ranging

Table 3
Electrical conductivity, activation energy and thermal expansion coefficient (TEC) of the investigated compositions

Sample number	Porosity/%	Electrical conductivity at 800°C in air/ S cm^{-1}		Activation energy/eV	TEC between 30°C and $800^\circ\text{C}/10^{-6} \text{K}^{-1}$
		Measured (effective)	Corrected (specific)		
001	44.4	30.8	99	0.10	12.2
020	65.6	8.2	70	0.18	11.7
021	53.2	8.7	40	0.20	12.3
022	45.7	26.9	91	S–M ^a	13.2
023	34.1	119.8	276	M ^b	13.6
024	52.0	15.3	66	S–M ^a	13.1
025	43.9	44.2	140	S–M ^a	13.3
026	37.0	68.6	172	S–M ^a	13.2
009	15.0	80.3	111	S–M ^a	11.6
010	44.4	0.5	1.6	0.48	11.4
011	27.7	7.7	14.8	0.27	10.5
012	36.9	23.1	58	0.19	12.3
027	56.3	15.7	82	S–M ^a	13.3
028	48.4	12.0	45	S–M ^a	13.0
029	56.8	2.6	13.9	0.15	11.5
030	56.4	2.9	15.1	0.16	12.3
031	50.6	18.8	77	S–M ^a	13.5
032	59.8	4.6	29	0.28	11.6
033	41.3	14.4	42	S–M ^a	12.5

^a S–M = transition from semiconducting to metallic conductivity with increasing temperature.

^b M = metallic conductivity in the whole temperature range.

from 1.6 S cm^{-1} to 276 S cm^{-1} and is in good agreement with literature data [1,2,15]. Tai et al. [1] obtained about 100 S cm^{-1} for $\text{La}_{0.8}\text{Sr}_{0.2}\text{FeO}_{3-\delta}$ after sintering at 1350°C , whereas the corrected conductivity is 111 S cm^{-1} . In the case of $\text{La}_{0.8}\text{Sr}_{0.2}\text{MnO}_{3-\delta}$, Ahlgren and Poulsen [15] and Kuo et al. [17] measured about 125 S cm^{-1} at 800°C , whereas the data correction of the highly porous $\text{La}_{0.8}\text{Sr}_{0.2}\text{MnO}_{3-\delta}$ sample resulted in 100 S cm^{-1} . These comparisons show that the data calculated using Eq. (1) have an error of about 10–30% depending on the remaining porosity of 15–60%. Because of the low sintering temperature of 950°C , which is representing a low sintering temperature of cathodes or a typical assembling temperature of an SOFC stack, the effective conductivity data are significantly lower than the corrected conductivity values. As a general observation from Eq. (1), the measured conductivity is only 15–25% and 35–50% of the specific conductivity, when the porosity is in the range of 50–60% and 30–40%, respectively. This has to be

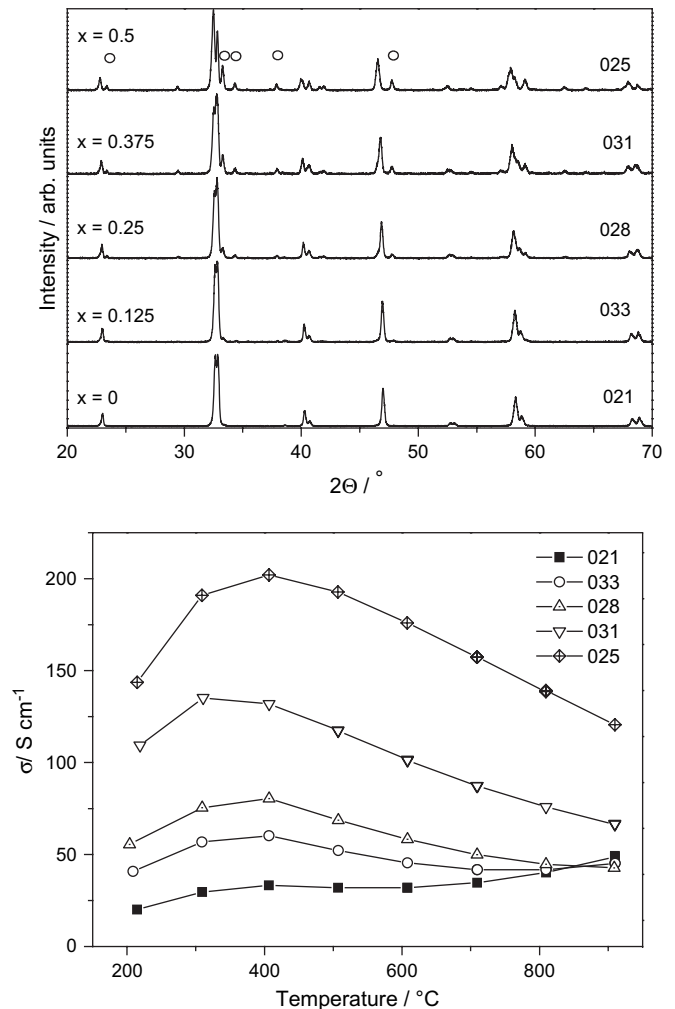


Fig. 3. XRD patterns after calcination at 950°C for 6 h in air (top) and the variation of the electrical conductivity between 200°C and 900°C (bottom) of samples 021, 033, 028, 031 and 025 in the $\text{La}_{0.8}\text{Sr}_{0.2}\text{Cu}_{0.5}\text{Mn}_{0.5-x}\text{Fe}_x\text{O}_{2.65+\delta}$ series ($x = 0, 0.125, 0.25, 0.375$ and 0.5 , respectively). Open circles in the XRD pattern indicate the positions for reflections of the tetragonal perovskite structure.

considered for applications of these materials when the heat treatment remains below 1000 °C.

In the quasi-binary system $\text{La}_{0.8}\text{Sr}_{0.2}\text{MnO}_{3-\delta}$ – $\text{La}_{0.8}\text{Sr}_{0.2}\text{FeO}_{3-\delta}$, the minimum conductivity of the quasi-ternary system was found for $\text{La}_{0.8}\text{Sr}_{0.2}\text{Fe}_{0.75}\text{Mn}_{0.25}\text{O}_{3-\delta}$. The highest σ in this quasi-binary system is 111 S cm^{-1} for $\text{La}_{0.8}\text{Sr}_{0.2}\text{FeO}_{3-\delta}$. Starting with these compositions and considering the addition of Cu, a gradual increase in the electrical conductivity is observed in the whole quasi-ternary system.

The activation energy of the electrical conductivity of some compositions was not calculated as they exhibited metallic conductivity (e.g. sample 023) or a transition from semiconducting to metallic behavior (Table 3). For the semiconducting compounds, the activation energy was calculated from the temperature dependence of the electrical conductivity ranging from 0.1 eV to 0.48 eV. Apparently, there is a correlation between the conductivity behavior and the crystallographic structures formed at each composition. Referring to Fig. 1, $\text{La}_{0.8}\text{Sr}_{0.2}\text{CuO}_{2.4+\delta}$ (sample 023) shows metallic conductivity and crystallizes as a single-phase tetragonal perovskite. All other compositions shown as filled squares in Fig. 1 exhibit a transition from semiconducting to metallic behavior and contain both tetragonal and hexagonal perovskites at room temperature. Only $\text{La}_{0.8}\text{Sr}_{0.2}\text{FeO}_{3-\delta}$ (also marked with a filled square) crystallizes as a single-phase orthorhombic perovskite. The remaining compositions (open circles) exhibit semiconducting behavior. Additionally, the varying ratio of main and secondary phases among the different compositions also seems to affect the electrical conductivity. The correlation between the XRD patterns and the electrical conductivity as

a function of the temperature of samples 021, 033, 028, 031 and 025 in the $\text{La}_{0.8}\text{Sr}_{0.2}\text{Cu}_{0.5-x}\text{Mn}_{0.5-x}\text{Fe}_x\text{O}_{2.65+\delta}$ series shown in Fig. 3 reveals that for a purely hexagonal perovskite as in sample 021 ($x=0$) the lowest conductivity is observed within this series (neglecting the data point at 900 °C). With increasing amount of tetragonal crystal phase, the conductivity increases over the whole temperature range. The higher the tetragonal phase content, the more pronounced is the inflection of the conductivity curve (transition from semiconducting to metallic behavior) at about 300–400 °C.

Analyzing the contour lines of the electrical conductivity values observed at 800 °C and presented in Fig. 4, a sharp increase in σ values is observed in the regions where semiconducting behavior is not dominant (Cu-rich region). For the Cu-poor compositions with $0 \leq \text{Cu} \leq 0.5$, the conductivity increases with increasing Cu content is very smooth for $\text{La}_{0.8}\text{Sr}_{0.2}\text{Mn}_{0.5-x/2}\text{Fe}_{0.5-x/2}\text{Cu}_x\text{O}_{2.9-x/2+\delta}$ and $\text{La}_{0.8}\text{Sr}_{0.2}\text{Mn}_{1-x}\text{Cu}_x\text{O}_{2.9-x/2+\delta}$, but much more pronounced for $\text{La}_{0.8}\text{Sr}_{0.2}\text{Fe}_{1-x}\text{Cu}_x\text{O}_{2.9-x/2+\delta}$.

3.3. Dilatometry

The thermal expansion coefficients (TEC) listed in Table 3 were determined in the temperature range between 30 °C and 800 °C in air and are schematically presented in a quasi-ternary plot in Fig. 5. The TEC values vary over a range from $10.5 \times 10^{-6} \text{ K}^{-1}$ for $\text{La}_{0.8}\text{Sr}_{0.2}\text{Fe}_{0.5}\text{Mn}_{0.5}\text{O}_{3-\delta}$ (sample 011) to $13.6 \times 10^{-6} \text{ K}^{-1}$ for $\text{La}_{0.8}\text{Sr}_{0.2}\text{CuO}_{2.4+\delta}$ (sample 023). It is interesting to note that the change of TEC for the quasi-binary compositions $\text{La}_{0.8}\text{Sr}_{0.2}\text{Mn}_{1-x}\text{Cu}_x\text{O}_{2.9-x/2+\delta}$ ($0.3 < x < 0.7$) remains constant when Mn and Cu are replaced by Fe. In other

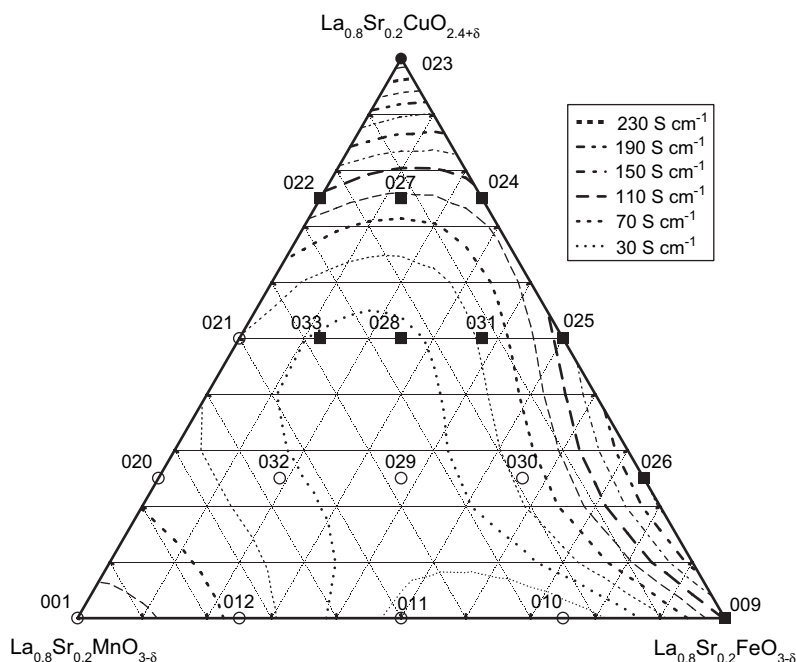


Fig. 4. Dependence of isothermal electrical conductivity at 800 °C in the quasi-ternary $\text{La}_{0.8}\text{Sr}_{0.2}\text{MnO}_{3-\delta}$ – $\text{La}_{0.8}\text{Sr}_{0.2}\text{CuO}_{2.4+\delta}$ – $\text{La}_{0.8}\text{Sr}_{0.2}\text{FeO}_{3-\delta}$ system measured in air. The lines correspond to a fitting of the experimental data with a full cubic function and have an interval of 20 S cm^{-1} . In the legend only the bold lines are listed. The symbols correspond to compositions with semiconducting electrical conductivity (open circles), with transition from semiconducting to metallic conductivity with increasing temperature (filled squares) and with metallic conductivity (filled circles), cf. Table 3.

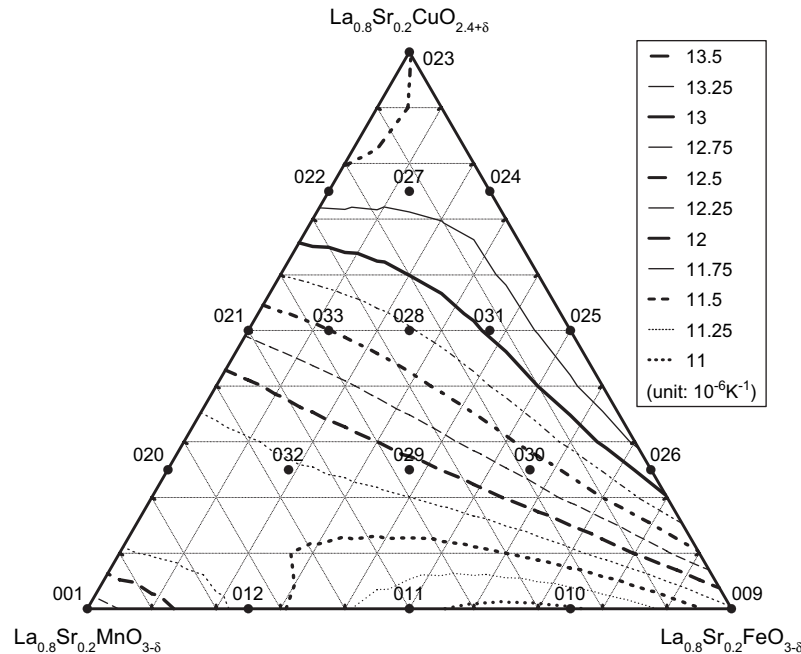


Fig. 5. Dependence of the thermal expansion coefficients between 30 °C and 800 °C in the quasi-ternary $\text{La}_{0.8}\text{Sr}_{0.2}\text{MnO}_{3-\delta}$ – $\text{La}_{0.8}\text{Sr}_{0.2}\text{CuO}_{2.4+\delta}$ – $\text{La}_{0.8}\text{Sr}_{0.2}\text{FeO}_{3-\delta}$ system. The lines correspond to a fitting of the experimental data with a full cubic function and have an interval of $0.25 \times 10^{-6} \text{ K}^{-1}$.

words, if the Cu/Mn ratio is kept constant, the substitution of Fe does not lead to a change of the TEC values. The variation of the thermal expansion coefficients in this quasi-ternary system appears to be exclusively dependent on the Cu/Mn ratio. Near to $\text{La}_{0.8}\text{Sr}_{0.2}\text{FeO}_{3-\delta}$ (sample 009) the contour lines of the TEC run approximately parallel to each other. A more detailed study of compositions within the Fe-rich vertex region is required to better resolve the TEC behavior.

4. Conclusions

Systematically selected compositions in the quasi-ternary $\text{La}_{0.8}\text{Sr}_{0.2}\text{MnO}_{3-\delta}$ – $\text{La}_{0.8}\text{Sr}_{0.2}\text{CuO}_{2.4+\delta}$ – $\text{La}_{0.8}\text{Sr}_{0.2}\text{FeO}_{3-\delta}$ system were synthesized by the Pechini method and characterized under identical conditions. X-ray diffraction data of these compositions are presented collectively thus enabling a schematic description of crystallographic phase distribution. The characteristic feature of this system is the appearance of tetragonal, hexagonal and orthorhombic perovskites, whereby the tetragonal and hexagonal phases often crystallize as a two-phase mixture.

The electrical conductivity values at 800 °C in air vary between 1.6 S cm^{-1} and 276 S cm^{-1} . The magnitude of the electrical conductivity of the perovskites is mainly determined by the percentage of Cu in the compositions. The lowest electrical conductivity values were measured in the $\text{La}_{0.8}\text{Sr}_{0.2}\text{MnO}_3$ – $\text{La}_{0.8}\text{Sr}_{0.2}\text{FeO}_3$ quasi-binary system.

The TECs between 30 °C and 800 °C in air are mainly determined by the Cu/Mn ratio in the compositions and vary

from 10.5 – $12.3 \times 10^{-6} \text{ K}^{-1}$ for $\text{La}_{0.8}\text{Sr}_{0.2}\text{Fe}_{1-x}\text{Mn}_x\text{O}_{3-\delta}$ to $13.6 \times 10^{-6} \text{ K}^{-1}$ for $\text{La}_{0.8}\text{Sr}_{0.2}\text{CuO}_{2.4+\delta}$.

Acknowledgments

Financial support from the German Federal Ministry of Economics and Technology is gratefully acknowledged. The authors thank P. Lersch for the XRD measurements, V. Bader for assistance with the sintering experiments, H. Lippert and N. Merki (FZJ-ZCH) for chemical analyses. In addition, the authors gratefully acknowledge Dr. J. L. Marqués-Lopéz for fruitful discussions.

References

- [1] L.-W. Tai, M.M. Nasrallah, H.U. Anderson, D.M. Sparlin, S.R. Sehlin, *Solid State Ionics* 76 (1995) 259.
- [2] E. Ivers-Tiffée, A. Weber, D. Herbstritt, *J. Eur. Ceram. Soc.* 21 (2001) 1805.
- [3] A. Petric, P. Huang, F. Tietz, *Solid State Ionics* 135 (2000) 719.
- [4] F. Riza, C. Ftikos, F. Tietz, W. Fischer, *J. Eur. Ceram. Soc.* 21 (2001) 1769.
- [5] P. Gordes, N. Christiansen, F.W. Poulsen, L. Bouakaz, K. Thomsen, in: F.W. Poulsen, N. Bonanos, S. Linderth, M. Mogensen, B. Zachau-Christiansen (Eds.), *Proceedings of the seventeenth Risø International Symposium on Materials Science*, Risø National Laboratory, Roskilde, Denmark, 1996, pp. 247–252.
- [6] G.C. Kostogloudis, C. Ftikos, *Solid State Ionics* 126 (1999) 143.
- [7] M. Zahid, I. Arul Raj, F. Tietz, P. Lersch, D. Stöver, in: S.C. Singhal, J. Mizusaki (Eds.), *Proceedings of the ninth International Symposium on Solid Oxide Fuel Cells (SOFC-IX)*, vol. 2, The Electrochemical Society, Pennington, NJ, USA, 2005, pp. 1708–1716.
- [8] Y. Khan, *J. Mater. Sci. Lett.* 6 (1987) 387.
- [9] C. Michel, L. Er-Rakho, B. Raveau, *Mater. Res. Bull.* 20 (1985) 667.
- [10] H.-C. Yu, K.-Z. Fung, *J. Power Sources* 133 (2004) 162.

- [11] S. Darracq, S.G. Kang, J.H. Choy, G. Demazeau, J. Solid State Chem. 114 (1995) 88.
- [12] M. Zahid, I. Arul Raj, W. Fischer, F. Tietz, J.M. Serra Alfaro, Solid State Ionics 177 (2006) 3205.
- [13] J.H. Kuo, H.U. Anderson, D.M. Sparlin, J. Solid State Chem. 83 (1989) 52.
- [14] F. Tietz, I. Arul Raj, M. Zahid, A. Mai, D. Stöver, Prog. Solid State Chem., doi:10.1016/j.progsolidstchem.2007.01.028.
- [15] E.O. Ahlgren, F.W. Poulsen, Solid State Ionics 86–88 (1996) 1173.
- [16] M.P. Pechini, U.S. Patent No. 3,330,697, 1967.
- [17] J.H. Kuo, H.U. Anderson, D.M. Sparlin, J. Solid State Chem. 87 (1990) 55.